Dynamic Contrast–Enhanced MRI of OATP Dysfunction in Diabetes

Dorela D. Shuboni-Mulligan,[1,2] Maciej Parys,[3] Barbara Blanco-Fernandez,[1,2] Christiane L. Mallett,[1,2] Regina Schnegelberger,[4] Marilia Takada,[3] Shatadru Chakravarty,[1,2] Bruno Hagenbuch,[4] and Erik M. Shapiro[1,2]

Diabetes 2019;68:271–280 | https://doi.org/10.2337/db18-0525

Diabetes is associated with hepatic metabolic dysfunction predisposing patients to drug-induced liver injury. Mouse models of type 2 diabetes (T2D) have dramatically reduced expression of organic anion transporting polypeptide (OATP)1A1, a transporter expressed in hepatocytes and in the kidneys. The effects of diabetes on OATP1B2 expression are less studied and less consistent. OATP1A1 and OATP1B2 both transport endogenous substrates such as bile acids and hormone conjugates as well as numerous drugs including gadoxetate disodium (Gd-EOB-DTPA). As master pharmacokinetic regulators, the altered expression of OATPs in diabetes could have a profound and clinically significant influence on drug therapies. Here, we report a method to noninvasively measure OATP activity in T2D mice by quantifying the transport of hepatobiliary-specific gadolinium-based contrast agents (GBCAs) within the liver and kidneys using dynamic contrast–enhanced MRI (DCE-MRI). By comparing GBCA uptake in control and OATP knockout mice, we confirmed liver clearance of the hepatobiliary-specific GBCAs, Gd-EOB-DTPA, and gadobenate dimeglumine, primarily though OATP transporters. Then, we measured a reduction in the hepatic uptake of these hepatobiliary GBCAs in T2D *ob/ob* mice, which mirrored significant reductions in the mRNA and protein expression of OATP1A1 and OATP1B2. As these GBCAs are U.S. Food and Drug Administration–approved agents and DCE-MRI is a standard clinical protocol, studies to determine OATP1B1/1B3 deficiencies in human individuals with diabetes can be easily envisioned.

Organic anion transporting polypeptides (OATPs) expressed on the sinusoidal surface of hepatocytes play a critical role in hepatic metabolism and physiology by mediating the uptake of an extensive array of endogenous substrates, such as bile acids, conjugated bilirubin, hormones, and their metabolites, and numerous drugs, such as antidiabetic agents (meglitinides and thiazolidinediones), statins, ACE inhibitors, chemotherapeutics, antibiotics, and certain imaging agents (1). Reduction in the expression or function of hepatic OATPs, due either to disease or pharmacologic inhibition, results in poor hepatic clearance of endogenous toxins, elevates plasma concentrations of drugs, and increases drug-induced adverse effects and complications in peripheral organs (2).

In rodent type 1 diabetes (T1D) models, including $Ins2^{Akita}$ mice and streptozotocin-treated rats, and in type 2 diabetes (T2D) models (*ob/ob* and *db/db* mice) the expression of influx and efflux transporters, as well as detoxification enzymes, are markedly decreased versus nondiabetic controls. A striking feature in these rodent diabetes models is near complete reduction of hepatic OATP levels, in particular OATP1A1 (Table 1). The effects of diabetes on OATP1B2 expression are less studied, and in those studies that have reported measurements, the findings are less consistent. It is unknown whether the expression of the functionally analogous human OATP1B1/B3 transporters is similarly reduced in patients with diabetes. There is, however, indirect

[1]Department of Radiology, Michigan State University, East Lansing, MI
[2]Institute for Quantitative Health Sciences and Engineering, Michigan State University, East Lansing, MI
[3]Department of Comparative Medicine and Integrative Biology Program, Michigan State University, East Lansing, MI
[4]Department of Pharmacology, Toxicology, and Therapeutics, University of Kansas Medical Center, Kansas City, MO

Corresponding author: Erik M. Shapiro, shapir86@msu.edu

Received 10 May 2018 and accepted 10 November 2018

This article contains Supplementary Data online at http://diabetes.diabetesjournals.org/lookup/suppl/doi:10.2337/db18-0525/-/DC1.

M.P. is currently affiliated with the Royal (Dick) School of Veterinary Studies and the Roslin Institute, Roslin, Midlothian, U.K.

© 2018 by the American Diabetes Association. Readers may use this article as long as the work is properly cited, the use is educational and not for profit, and the work is not altered. More information is available at http://www.diabetesjournals.org/content/license.

Table 1—Diabetes-associated alterations of OATP1A1 and OATP1B2 expression in rodents

			OATP1A1		OATP1B2		
Species	Strain	Diabetes	Protein	RNA	Protein	RNA	Reference number
Mouse	*ob/ob*	T2D genetic	↓	↓	♀ ↑ ♂ =	♀ ↓ ♂ =	35
Mouse	*ob/ob*	T2D genetic	ND	↓	ND	=	36
Mouse	*ob/ob*	T2D genetic	↓	↓	ND	↓	37
Mouse	*db/db*	T2D genetic	↓	↓	♀ ↓ ♂ =	=	38
Mouse	C57BL/6	T2D induced	↓	=	=	=	39
Mouse	$Ins2^{Akita}$	T1D genetic	↓	↓	ND	=	40
Rat	Wistar	T1D induced	ND	↓	ND	ND	41

↓, decreased expression with diabetes; ↑, increased expression with diabetes; =, equal expression with diabetes; ND, no data.

evidence that predicts a downregulation of OATP expression in humans. The transcriptional pathways governing OATP expression are reduced in response to hyperglycemia (3), and patients with diabetes show reduced hepatic statin uptake, which is consistent with OATP1B1/B3 downregulation (4). Such OATP downregulation could profoundly influence drug therapy in individuals with diabetes, such as, for example, statin treatment for hyperlipidemia.

A key barrier to measuring hepatic transporter levels in patients with diabetes is the challenge of obtaining liver tissue for ex vivo assays. Hepatic OATPs transport numerous imaging agents into hepatocytes. Among them are two MRI gadolinium-based contrast agents (GBCAs), gadoxetate disodium (Gd-EOB-DTPA) (5,6) and gadobenate dimeglumine (Gd-BOPTA) (7,8). This enables the use of dynamic contrast–enhanced MRI (DCE-MRI) to characterize this uptake and provides quantitative assessment of hepatic and renal function. DCE-MRI has been used to study the impact of several diseases, including fibrosis (9), cirrhosis (10), viral hepatitis (11), drug-induced liver injury (12), and nonalcoholic fatty liver disease (NAFLD) (13), on hepatic function. Fibrosis and cirrhosis have received the most attention, and modeling DCE-MRI data has been expanded beyond rodents into the clinic (14,15). Several studies have demonstrated a clear relationship between OATP expression and pharmacokinetic changes of contrast agent dynamics (16,17); however, the use of DCE-MRI to measure changes in hepatic OATP expression in diabetes has not been reported.

The current study is the first report of the use of MRI to measure OATP reduction in diabetic animal models. First, we confirmed that OATPs are responsible for the majority of the hepatobiliary influx of Gd-EOB-DTPA and Gd-BOPTA in vivo. Then, we measured the reduction in the hepatic uptake of these hepatobiliary GBCAs in T2D *ob/ob* mice, which mirrored significant reductions in the mRNA and protein expression of OATP1A1 and OATP1B2. Because others have demonstrated the ease of transition from preclinical studies to the clinic with other liver-specific diseases using DCE-MRI, the application of the technique to monitor human diabetes is easy to envision.

RESEARCH DESIGN AND METHODS

In Vivo DCE-MRI General Protocol

Animal studies were approved by the Institutional Animal Care and Use Committee at Michigan State University and were performed in accordance with the National Institutes of Health *Guide for the Care and Use of Laboratory Animals* (NIH publication no. 80–23). Prior to imaging, animals were weighed and then anesthetized to place a tail vein catheter. The catheter was 80 cm long, which allowed for contrast injection during data acquisition, and was constructed of polyethylene tubing (PE-10) and 30-gauge needles. Animals were placed supine on a 2 × 2 surface receive array within a volume transmit coil. Body temperature and respiration were monitored (SA Instruments, Inc., Stony Brook, NY) and maintained at 33.5 ± 0.5°C and ~30 bpm. Images were acquired with a 7-T Bruker Biospec 70/30 USR using a RAREst sequence (echo time 4.66 ms; repetition time 200 ms; 200 × 200 μm) for 1 h (60 repetitions). Three different contrast agents were used: Gd-EOB-DTPA (Eovist), Gd-BOPTA (MultiHance), and gadopentetate dimeglumine (Gd-DTPA) (Magnevist). Gd-EOB-DTPA and Gd-BOPTA are hepatobiliary GBCAs, whereas Gd-DTPA is a negative control. Contrast agents (25 mg gadolinium/kg) were given in a bolus after three baseline scans and were each administered to all animals with 3–4 days between injections.

The Contribution of OATP in Hepatospecific GBCA Uptake In Vivo

Animals with the deletion of five *Slco1a* and *1b* genes, OATP1a/1b Cluster Knockout ($Slco1a/1b^{-/-}$) mice, were compared with appropriate controls, FVB mice (n = 5/group; Taconic Biosciences, Germantown, NY). This comparison allows for the first in vivo verification of OATP transport of hepatobiliary GBCA into the livers of rodents. Animals were scanned using the general protocol outlined above. At the completion of the experiment, animals were euthanized via exsanguination, and livers were collected and snap frozen with liquid nitrogen.

Effects of T2D on Hepatospecific GBCA Uptake In Vivo

B6.Cg-Lep^{ob}/J mice (*ob/ob* mice; The Jackson Laboratory, Bar Harbor, ME) were compared with age-matched

controls, C57BL/6 mice (n = 5/group), to determine the impact of T2D on liver and kidney function. Comparing the uptake of hepatobiliary contrast agents between groups gives insight into liver function, reflecting hepatic OATP concentration and its relationship with disease. Animals underwent the DCE-MRI protocol described above. At the completion of the experiment, animals were fasted for 12 h and then euthanized via exsanguination; blood samples were collected for insulin measurement. Body weights and individual organ (heart, liver, kidney, and pancreas) weights were measured for comparison. Liver tissue samples were snap frozen for quantitative PCR (qPCR) and Western analysis (five mice/group); additionally, liver and kidney samples (two mice/group) were preserved in 10% formalin for histology.

Characterization of T2D Mice

Blood samples were collected from the saphenous vein of animals using a 27-gauge needle, and blood glucose levels were measured using a commercially available glucometer (CONTOUR; Ascensia Diabetes Care). Blood glucose levels were measured to verify T2D at the completion of the experiment in animals fasted for 12 h. Insulin levels were measured using a commercially available ultrasensitive mouse insulin ELISA kit (Crystal Chem Inc., Elk Grove Village, IL). Blood (~1 mL) was collected from animals anesthetized under isoflurane, via terminal cardiac puncture using a heparinized syringe. Samples were spun at 2,000g at 4°C for 20 min to isolate plasma. Using 5 μL of sample, the groups were analyzed with the wide-range assay (0.1–12.8 ng/mL). Plates were read with a SpectraMax 190 Plate Reader (Molecular Devices, San Jose, CA). To examine the morphology and health of livers and kidneys, the two organs that excrete hepatobiliary GBCAs, organs from two animals for each group were collected and fixed in 10% formalin for at least 24 h. Organs were dehydrated, paraffin embedded, and sectioned at 10 μm. Tissue was then stained for hematoxylin-eosin and the slides were imaged using a Leica DMI4000B Microscope and the Leica Application Suite.

Measurements of mRNA and Protein Expression of OATP1A1 and OATP1B2 in Mouse Cohorts

OATP1A1 and OATP1B2 protein levels were measured using Western blot. Membrane proteins were isolated from 138 to 236 mg of liver tissue using a Teflon tissue grinder (Wheaton, Millville, NJ) and 3 mL of hypotonic homogenization solution (1 mmol/L NaCl, 5 mmol/L Tris-HCl; pH 7.5) (Complete Protease Inhibitor Cocktail; Sigma-Aldrich, St. Louis, MO). Samples were homogenized on ice with 20 strokes and then centrifuged for 10 min at 900g and 4°C. The supernatants were then centrifuged again for 20 min at 10,000g and 4°C to yield a protein pellet. Total protein levels were quantified using a BCA Protein Assay Kit. Samples (50 μg protein) were loaded into 4–20% Mini-PROTEAN TGX precast protein gels (Bio-Rad Laboratories, Hercules, CA). After electrophoresis, proteins were transferred to polyvinylidene fluoride membranes and blocked for 1 h with TBS Odyssey Blocking Buffer (LI-COR, Lincoln, NE) for the OATP1A1 blots or with 5% nonfat milk in Tris-buffered saline with Tween for the OATP1B2 blots. Membranes were then incubated with antibodies against OATP1A1 (1:2,000) (provided by Dr. B. Stieger, University Hospital Zurich, Switzerland) and Na^+/K^+ ATPase (1:1,000) (ab7671; Abcam) overnight at 4°C or OATP1B2 (1:1,000) (Genscript, Piscataway, NJ) and β-actin (1:10,000) (A5441; Sigma-Aldrich) for 1 h at room temperature. After three washes with Tris-buffered saline with Tween, OATP1A1 membranes were incubated with two secondary antibodies, IRDye 800CW goat anti-rabbit (1:15,000) (LI-COR) and IRDye 680LT goat anti-mouse (1:20,000) (LI-COR), whereas OATP1B2 membranes were incubated with a horseradish peroxidase–conjugated goat anti-rabbit antibody (1:10,000) (Thermo Fisher Scientific, Waltham, MA) and the IRDye 680LT goat anti-mouse (1:20,000) (LI-COR) for 1 h at room temperature in Casein Odyssey Blocking Buffer (LI-COR). Images were then acquired using an Odyssey Fc imaging system (LI-COR) and signal intensity for OATP1A1, OATP1B2, Na^+/K^+ ATPase, and β-actin bands was measured for all mice (Image Studio Software; LI-COR). Total signal for each animal was calculated by dividing the OATP1A1 signal by the Na^+/K^+ ATPase signal or the OATP1B2 signal by the β-actin signal.To determine the RNA levels of *Slco1a1* in the livers of diabetic animals, qPCR analysis was performed comparing C57BL/6 and *ob/ob* mice. RNA was isolated from frozen livers using hard tissue an Omni Tip homogenizer (Omni International, Kennesaw, GA) and a commercially available RNA extraction kit (Thermo Fisher Scientific). After isolation, we quantified RNA levels using a Qubit 2.0 Fluorometer and the Qubit RNA assay kit. Reverse transcription was performed using Superscript III with random primer hexamers according to manufacturer recommendations. To measure *Slco1a1* at the transcriptional level, qPCR was performed using TaqMan assays with previously validated primer sets (Thermo Fisher Scientific). Assays were performed on a StepOnePlus Real-Time PCR System (Applied Biosystems, Foster City, CA). GAPDH (Applied Biosystems) was used as an endogenous control, and we assessed liver gene expression differences between the normal mice and diabetic mice with the ddCT method.

Statistical Analysis

Raw MRI signal intensity data within regions of interest (liver and kidney) were extracted from magnetic resonance images using the Image Display tool in Paravison 6.0 (Bruker). We exported these data into Excel (Microsoft) and calculated the percentage of signal enhancement (PSE) at each time point, normalized to precontrast enhancement

$$\left(\frac{Value - \overline{Baseline}}{\overline{Baseline}}\right) * 100 = PSE.$$

The area under the curve (AUC) was calculated using the trapezoidal method to determine the percentage of

clearance by organ. The values were then statistically compared across groups using two-way mixed-model ANOVA, with within-subject groups for the contrast agents and between-subject experimental groups for the mouse type.

To compare physiological effects of diabetes, we used independent samples *t* tests to determine differences between T2D and control mice.

RESULTS

The Contribution of OATP in Hepatospecific GBCA Uptake In Vivo

To monitor the direct impact of OATPs on the hepatic uptake of GBCAs in vivo, DCE-MRI was performed in *Slco1a/1b*$^{-/-}$ mice. Figure 1 shows serial in vivo MRI of FVB control mice and *Slco1a/1b*$^{-/-}$ mice after Gd-EOB-DTPA injection. Livers and kidneys for both mouse groups appear dark in baseline images prior to the injection of agent, which was administered at t = 0. Within the first minute, increases in PSE due to the contrast agent are observed in the blood vessels in the liver and diffusely within the entire kidneys of both groups. At 2 min postinjection, the kidneys in both groups reached peak PSE. At this time point, the difference in signal enhancement in the liver becomes clear between the two groups. Control FVB mice have increased signal intensity in the liver, whereas *Slco1a/1b*$^{-/-}$ mice have no enhancement within the liver. By 5 min postinjection, the liver in FVB mice has reached peak PSE and loses signal intensity with increasing time. Additionally, the spatial distribution of signal enhancement within the kidney cortex of FVB and *Slco1a/1b*$^{-/-}$ mice was different than that of C57BL/6 mice observed in the subsequent study, suggesting a difference in kidney clearance between strains (Supplementary Fig. 1).

The PSE as a function of time for each agent in the liver and kidneys is shown in Fig. 2*A*. Liver signal enhancement was markedly different between FVB and *Slco1a/1b*$^{-/-}$ mice. In FVB mice, Gd-EOB-DTPA and Gd-BOPTA had 119% and 210% PSE compared with baseline, respectively. *Slco1a/1b*$^{-/-}$ mice had lower peak PSE, 24.1% for both Gd-EOB-DTPA and Gd-BOPTA. Gd-DTPA injections had similarly low PSE for both FVB and Slco1a/1b$^{-/-}$ mice. The nonhepatospecific contrast agent Gd-DTPA is eliminated solely through the kidney, and no enhancement is seen in the liver in either FVB or *Slco1a/1b*$^{-/-}$ mice. General kidney signal enhancement profiles were similar between the two groups, with Gd-BOPTA and Gd-DTPA having higher maximum PSE than Gd-EOB-DTPA. However, the PSE was higher in FVB mice (Gd-BOPTA, 234.2%; Gd-DTPA, 190.4%; Gd-EOB-DTPA, 97.9%) than *Slco1a/1b*$^{-/-}$mice (Gd-BOPTA, 119.1%; Gd-DTPA, 126.5%; Gd-EOB-DTPA, 55.0%).

AUC analysis enabled statistical comparison between the different agents and experimental groups for the liver and kidney (Fig. 2*B*). There were significant main effects of both agent ($F(2,16) = 39.9$, $P < 0.001$) and mouse type ($F(1,8) = 36.7$, $P < 0.001$), and an interaction between agent and mouse type ($F(2,16) = 251.1$, $P < 0.001$). All agents had a significant difference between the FVB and *Slco1a/1b*$^{-/-}$ mice, but the differences were larger for Gd-EOB-DTPA and Gd-BOPTA. Kidney AUCs had one significant main effect for agent ($F(2,16) = 14.3$, $P < 0.001$) and no main effect for experimental group ($F(1,8) = 2.6$, $P = 0.146$) or interaction ($F(2,16) = 0.357$, $P = 0.705$). Gd-BOPTA and Gd-DTPA both had significantly higher AUCs than Gd-EOB-DTPA. The liver and kidney AUCs were then used to calculate the percentage of clearance by organ (Fig. 2*C*); liver AUC was divided by the sum of liver plus kidney AUCs and multiplied by 100. To analyze the data, an arcsine transformation was performed to correct the percentage values and allow for statistical comparison. Significant main effects were found for both agent ($F(2,16) = 19.9$, $P < 0.001$) and mouse type ($F(1,8) = 208.3$, $P < 0.001$), as well as an interaction between agent and mouse type ($F(2,16) = 15.3$, $P < 0.001$). This comparison corrected for the lower contrast enhancement produced in Gd-EOB-DTPA compared with Gd-BOPTA and Gd-DTPA. FVB mice had statistically similar total clearance by the liver for Gd-EOB-DTPA (47%) and Gd-BOPTA (57%); these values were both significantly different than all other values (13.3–9.4%).

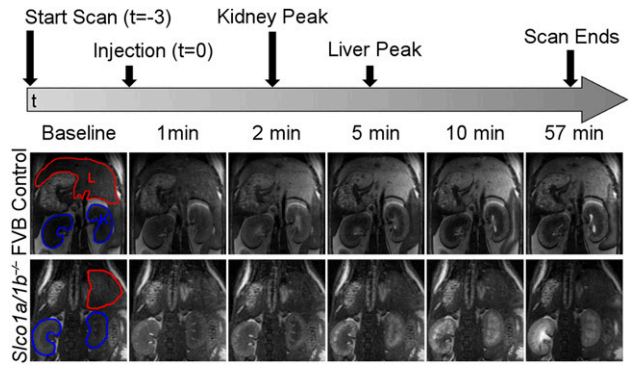

Figure 1—DCE-MRI of FVB control and *Slco1a/1b*$^{-/-}$ mice after Gd-EOB-DTPA injection. The top panel depicts a schematic of the MRI protocol, including the time of injection and the peaks in signal enhancement for both regions of interest (ROIs). The bottom panel demonstrates magnetic resonance images across the time course for FVB control and *Slco1a/1b*$^{-/-}$ mice. The baseline images have the ROI outlined, with liver (L) in red and kidney (K) in blue.

Characterization of T2D Mice

We verified the T2D model, demonstrating differences in both physiology and molecular expression of the disease in *ob/ob* mice when compared with controls. The *ob/ob* mice had significantly increased body weight and liver weight with no difference in heart and kidney weights, similar to previous publications (Table 2) (18,19). Typical for the strain, histology of the liver demonstrates alteration in hepatocyte morphology and the development of steatosis (Fig. 3*A*) caused by excessive food intake (20,21). The *ob/ob* mice also had significantly elevated levels of fasting blood glucose ($t(7) = 4.515$, $P = 0.003$) (Supplementary Fig. 2*A*) and are hyperinsulinemic ($t(7) = 2.961$, $P = 0.025$) (Supplementary Fig. 2*B*).

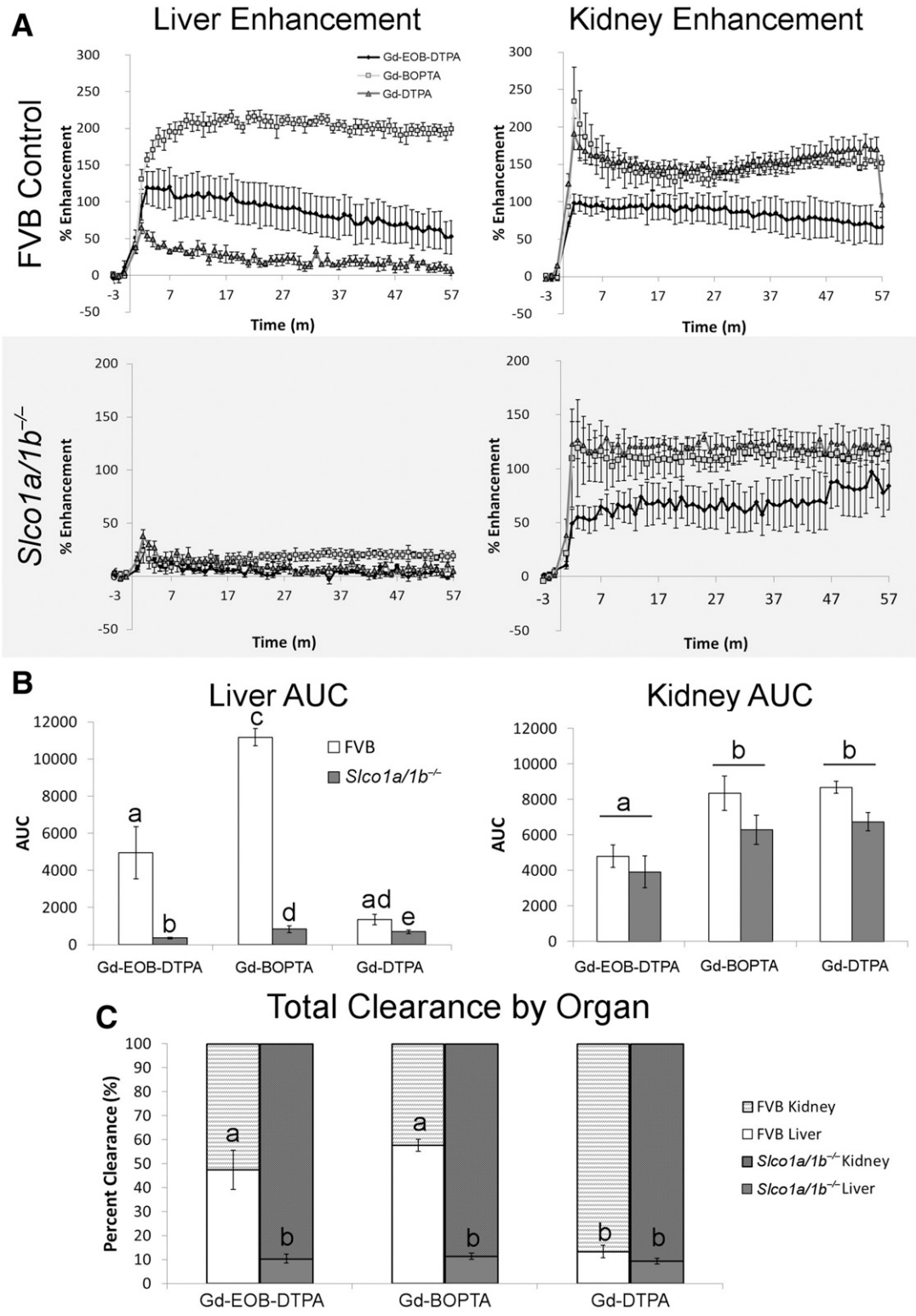

Figure 2—Quantitative analysis of DCE-MRI data for FVB control and *Slco1a/1b*$^{-/-}$ mice. *A*: PSE for the liver (left) and kidney (right) for FVB (top panel) and *Slco1a/1b*$^{-/-}$ mice (gray; bottom panel). Lines within the graph represent the contrast agent administered: Eovist (black diamond), MultiHance (light gray square), and Magnevist (dark gray triangle). m, minutes. *B*: AUC for liver (left) and kidney (right), with white bars representing FVB mice and dark gray representing *Slco1a/1b*$^{-/-}$ mice. Different letters represent significant differences between each mean (liver) or contrast agent (kidney), $P < 0.05$. *C*: Total clearance by organ after the administration of the three contrast agents is represented as a percentage of clearance for the liver (bottom bar) and kidney (top bar). Different letters represent significant differences between each mean, $P < 0.05$.

Table 2—Weight differences between C57BL/6 and *ob/ob* mice for various organs

	Body weight (g)	Heart weight (g)	Liver weight (g)	Kidney weight (g)
C57BL/6	31.20 ± 0.49	0.17 ± 0.01	1.21 ± 0.03	0.38 ± 0.02
ob/ob	53.50 ± 3.84*	0.17 ± 0.01	3.42 ± 0.31*	0.38 ± 0.05

Data are presented as the mean ± SEM. *$P < 0.05$ compared with C57BL/6 mice.

Effects of T2D on Hepatospecific GBCA Uptake In Vivo

To determine the effects of decreased hepatic OATP levels in T2D mice, we examined the clearance of hepatospecific GBCAs in vivo for *ob/ob* mice. Figure 4 shows in vivo MRI of the livers and kidneys for C57BL/6 control and *ob/ob* mice preinjection and postinjection of the three contrast agents, Gd-EOB-DTPA, Gd-BOPTA, and Gd-DTPA. Baseline images prior to the injection of the agent show dark liver and kidneys in both C57BL/6 and *ob/ob* mice. By 5 min postinjection, the liver reached peak PSE for both groups of mice when given either Gd-EOB-DTPA or Gd-BOPTA. No liver enhancement is observed for the nonhepatospecific control GBCA Gd-DTPA in either control or *ob/ob* mice.

The PSE as a function of time for each agent in the liver and kidneys are shown in Fig. 5*A*. Gd-EOB-DTPA shows lower peak PSE for livers and higher peak PSE in kidneys of *ob/ob* mice (liver, 72.2%; kidney, 138.9%) compared with C57BL/6 controls (liver, 107.9%; kidney, 68.3%). Similar differences in the peak PSE between *ob/ob* (liver, 142.9%; kidney, 160.5%) and C57BL/6 (liver, 72.0%; kidney, 246.8%) mice were observed for Gd-BOPTA. For Gd-DTPA, both C57BL/6 and *ob/ob* mice had similar low levels of peak liver PSE (C57BL/6, 41.4%; *ob/ob*, 46.9%) and high levels of peak kidney PSE (C57BL/6, 163.1%; *ob/ob*, 219.6%).

AUC analysis allowed for the statistical comparison of the different agents and mouse type for the liver and kidney (Fig. 5*B*). Liver AUCs have significant main effects of both agent ($F(2,16) = 18.8$, $P < 0.001$) and mouse type ($F(1,8) = 5.9$, $P = 0.021$) and interaction between agent and mouse type ($F(2,16) = 11.9$, $P = 0.018$). The liver AUC for Gd-BOPTA of C57BL/6 mice had higher values than the other conditions. Kidney AUCs had two significant main effects for agent ($F(2,16) = 17.5$, $P < 0.001$) and mouse type ($F(1,8) = 12.54$, $P = 0.017$) but no interaction ($F(2,16) = 0.466$, $P = 0.641$). When the agent main effects were broken down, we found that Gd-BOPTA and Gd-DTPA both had significantly higher AUCs in the kidney compared with Gd-EOB-DTPA, similar to what we found for kidney AUC in the *Slco1a/1b*$^{-/-}$ experiment. However, there was also a main effect for mouse type, which showed a significantly higher kidney AUC value for *ob/ob* mice than C57BL/6 mice. The liver and kidney AUCs were then used to calculate the percentage of clearance by organ (Fig. 5*C*), as described above. Significant main effects were found for both agent ($F(2,16) = 72.3$, $P < 0.001$) and mouse type ($F(1,8) = 423.6$, $P < 0.001$), as well as an interaction

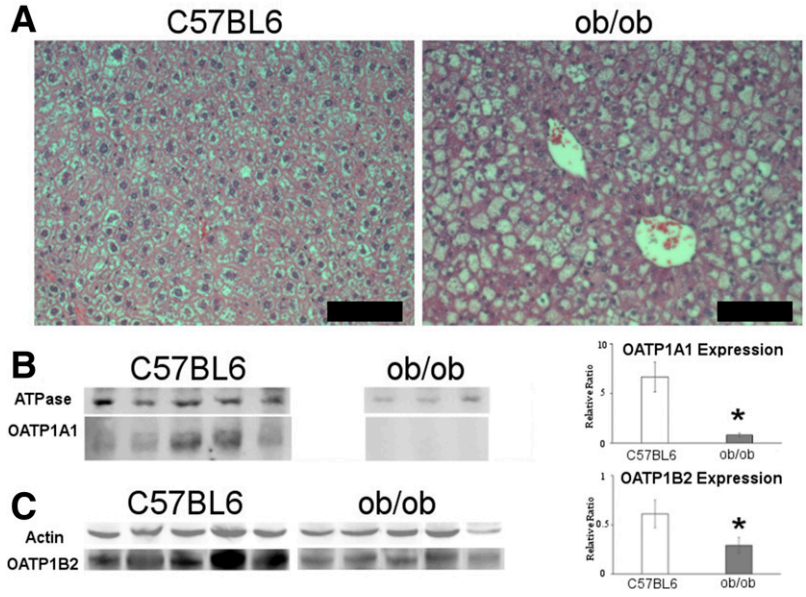

Figure 3—Characterization of T2D mice using histology and Western blot. *A*: Representative images of hematoxylin-eosin–stained liver sections for C57BL/6 (left) and *ob/ob* (right) mice. Scale bars = 50 μm. *B*: Fluorescent Western blot of C57BL/6 (left) and *ob/ob* (right) mice with Na^+/K^+ ATPase and OATP1A1. Graph represents the relative ratio OATP1A1 (Na^+/K^+ ATPase). *C*: Fluorescent/chemiluminescent Western blot of C57BL/6 (left) and *ob/ob* (right) mice with actin and OATP1B2. Graph represents the relative ratio of OATP1B2/(actin). *$P <$ 0.05, within graphs representing statistical significance.

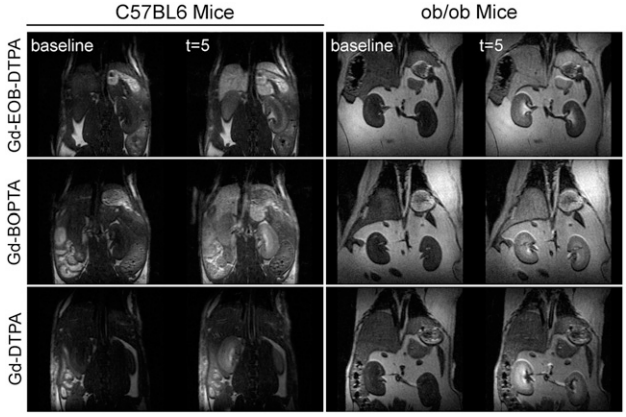

Figure 4— DCE-MRI of C57BL/6 and *ob/ob* mice before and after the injection of three difference contrast agents. The columns represent the two mouse types (C57BL/6 and *ob/ob*), whereas the rows are the different agents (Gd-EOB-DTPA, Gd-BOPTA, and Gd-DTPA). Each panel has an image acquired during baseline (left) and an image 5 min postinjection (t = 5; right).

between agent and mouse type ($F(2,16) = 4.488$, $P = 0.041$). The liver clearance of *ob/ob* mice after injection of the two hepatospecific contrast agents was significantly reduced compared with that of C57BL/6 mice, but was still higher than the clearance of Gd-DTPA.

Measurements of mRNA and Protein Expression of OATP1A1 and OATP1B2 in Mouse Cohorts

Quantitative PCR revealed a 12.7-fold reduction in the mRNA expression of *Slco1a1* in *ob/ob* mice. OATP1A1 protein content is displayed as a relative ratio, normalized to the level of the Na^+/K^+ ATPase signal. The *ob/ob* mice had levels that were 8.4 times lower than those for control C57BL/6 mice ($t(9) = 3.089$, $P = 0.013$). OATP1B2 protein content is displayed as a relative ratio, normalized to the level of the β-actin signal. The *ob/ob* mice had levels that were 2.1 times lower than those of the control C57BL/6 mice ($t(8) = 4.563$, $P = 0.002$).

DISCUSSION

In this study, we used a clinically translatable MRI protocol to measure hepatic dysfunction in a mouse model of T2D. First, we confirmed that hepatic OATPs are responsible for the uptake of hepatospecific GBCAs. Then, we used DCE-MRI to measure dysfunction in the hepatic uptake of hepatospecific GBCAs in a mouse model of T2D. The MRI results coincide with large reductions in hepatic OATP expression levels. The procedures detailed herein used U.S. Food and Drug Administration–approved MRI contrast agents and routine DCE-MRI imaging protocols amenable to performing studies in humans.

Available evidence from case studies suggests that OATPs are reduced in human individuals with diabetes, but these measurements have not been made. For example, Dostalek et al. (4) found in patients with diabetes reduced clearance of statins and statin metabolites, which are normally cleared from the blood by hepatic OATPs. However, the authors did not assess the responsible mechanism. Additionally, two articles previously published (22,23) reported that incidences of statin-induced myopathy are increased nearly 50-fold in individuals with diabetes versus individuals without diabetes, but they did not determine whether altered OATP expression contributed to this problem. Such variable responses and adverse effects of statins are known complications of diabetes, and although their mechanisms are not yet identified, they are consistent with reduced hepatic OATP expression or function. In addition to diabetes, other liver diseases such as cholestasis, drug-induced liver injury, and inflammation result in reduction of OATP levels, mediated by the downregulation of HNF-1α (24). Because of technical barriers, the concentrations of hepatic OATP genes or proteins expressed in human patients in vivo cannot be directly measured or inferred via any established biomarkers in blood or urine tests, and liver biopsy is highly invasive and too high risk and impractical for research or routine clinical use. The DCE-MRI procedure detailed in this study could be adopted to conduct meaningful clinical studies and/or to surveil patients with diabetes.

The findings that OATP1A1 and OATP1B2 levels are reduced in the *ob/ob* mouse model that was used is significant, because there are human ortholog transporters of the same families found in the liver: OATP1A2 and OATP1B1, and OATP1B3, respectively. OATP1A2 is not expressed in human hepatocytes; rather, it is expressed on the apical (biliary) membrane of cholangiocytes (25) and elsewhere throughout the body. In contrast, OATP1B1 and OATP1B3 are expressed on the sinusoidal (basolateral) membrane of hepatocytes, and both play a critical role in hepatic metabolism and physiology by mediating the hepatic uptake of an extensive array of endogenous substrates and also medically significant drugs. Both have demonstrated uptake of MRI contrast agents. Therefore, from a translational perspective, the data on OATP1B2 presented here are most relevant.

However, there are functional differences between human and rodent OATPs in the transport of the liver GBCAs used within our study. In cell culture experiments with cells expressing either OATP1A1 or OATP1B2, efficient transport of both hepatospecific MRI contrast agents, Gd-EOB-DTPA and Gd-BOPTA, is exhibited (5–7,26). However, in similar studies (27,28) within human embryonic kidney cells stably transfected with OATP1B1 or OATP1B3, only OATP1B1 and OATP1B3 efficiently transport Gd-EOB-DTPA. No such studies with OATP1B1 or OATP1B3 have been conducted with Gd-BOPTA (29), although it is known that after i.v. administration to humans, the clearance of Gd-BOPTA exhibits ~5% clearance by the liver and 95% clearance by the kidney (30), whereas in rodents, clearance by the liver is much higher (31.5–43%) (31,32). All publications with patients that

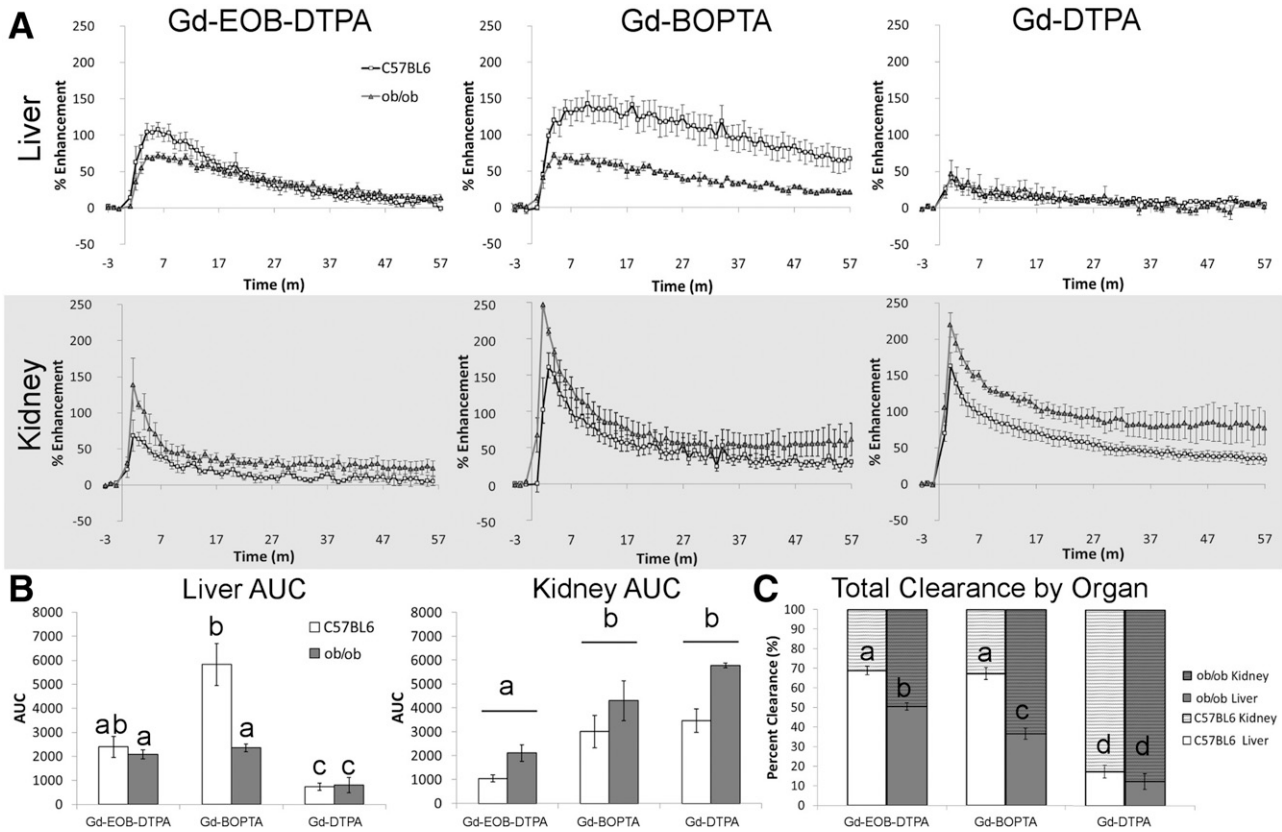

Figure 5—Quantitative analysis of DCE-MRI data for C57BL/6 control and *ob/ob* mice. *A*: PSE for the liver (top) and kidney (gray bottom) for the three different contrast agents: Gd-EOB-DTPA (left), Gd-BOPTA (middle), and Gd-DTPA (right). Lines within the graph represent the mouse type: C57BL/6 (white square) and *ob/ob* (dark gray triangle). m, minutes. *B*: AUC for liver (left) and kidney (right), with white bars representing C57BL/6 mice and dark gray bars representing *ob/ob* mice. Different letters represent significant differences between each mean (liver) or contrast agent (kidney), $P < 0.05$. *C*: Total clearance by organ after the administration of the three contrast agents is represented as a percentage of clearance for the liver (bottom bar) and kidney (top bar). Different letters represent significant differences between each mean, $P < 0.05$.

measured hepatocyte uptake of GBCAs, therefore, used Gd-EOB-DTPA to observe the liver difference between individuals with disease and healthy individuals.

Estimating liver function using DCE-MRI within rodent disease models and human patients has been implemented for both fibrosis and cirrhosis. OATP1A1 measurements in rodents with induced fibrosis caused by carbon tetrachloride have a significant twofold to threefold decrease in transporter transcription (16,17), which was also significantly correlated with all of the MRI parameters examined (16). OATP1B2 was not examined in that study. Another model of mouse fibrosis induced by NAFLD has also been shown to have altered liver GBCA uptake with DCE-MRI (13,33). NAFLD is highly comorbid with T2D, because steatosis is observed within the liver, which is similar to our findings in *ob/ob* mice (Fig. 3*A*) in ~70% of individuals with diabetes (34). Norén et al. (15) used Gd-EOB-DTPA–enhanced MRI to classify patients with NAFLD by the stages of fibrosis. It is therefore easy to envision a similar step into the clinic with individuals with diabetes, because diabetic mice have both a reduced transporter expression and visible alterations in DCE-MRI kinetics.

It is also worth considering these findings in the context of clinical MRI evaluations of liver function in patients with diabetes, for conditions other than diabetes itself, such as hepatic steatosis, fibrosis, and cirrhosis. Extracellular MRI contrast agents, used for perfusion imaging to elicit their image-contrasting properties in the blood and liver parenchyma, would not be sensitive to the OATP reduction in diabetes. The intracellular targeted contrast agents, such as Eovist, find their most important use after internalization into hepatocytes via OATPs, and as such they would be sensitive to this reduction. Thus, DCE-MRI evaluation of diseases such as NAFLD, fibrosis, and cirrhosis, using hepatospecific MRI contrast agents such as Eovist, may be convoluted by possible hepatic OATP reduction resulting from diabetes. To our knowledge, this complication has not been previously described and is critical to accurate measurements of liver function in patients with these comorbidities.

Conclusion

The current study is the first report of the use of MRI to measure OATP reduction in diabetic animal models.

Additionally, we confirmed that OATPs are responsible for the majority of in vivo hepatobiliary influx of Gd-EOB-DTPA and Gd-BOPTA in mice. Then, we measured a reduction in the hepatic uptake of these hepatobiliary GBCAs in T2D *ob/ob* mice, which mirrored significant reductions in the mRNA and protein expression of OATP1A1 and OATP1B2. Because these GBCAs are U.S. Food and Drug Administration–approved agents and DCE-MRI is a standard clinical protocol, studies to determine OATP1B1/B3 status in human individuals with diabetes can easily be envisioned.

Acknowledgments. The authors thank Dr. Bruno Stieger (University Hospital Zurich, Switzerland) for sharing the antibodies for OATP1A1 Western blot analysis.

Funding. B.H. was supported by the National Institutes of Health (NIH)/National Institute of General Medical Sciences (grant 5R01-GM-077336). E.M.S. received support from the NIH/National Institute of Diabetes and Digestive and Kidney Diseases (grant R01-DK-107697).

Duality of Interest. No potential conflicts of interest relevant to this article were reported.

Author Contributions. D.D.S.-M., B.H., and E.M.S. designed the study, performed experiments, analyzed data, and wrote the manuscript. M.P., B.B.-F., C.L.M., R.S., M.T., and S.C. performed experiments and reviewed/edited the manuscript. E.M.S. is the guarantor of this work and, as such, had full access to all the data in the study and takes responsibility for the integrity of the data and the accuracy of the data analysis.

Prior Presentation. Parts of this study were presented in abstract form at the 25th Annual International Society for Magnetic Resonance in Medicine, Honolulu, HI, 22–27 April 2017, and the World Molecular Imaging Congress, New York, NY, 7–10 September 2016.

References

1. Hagenbuch B, Stieger B. The SLCO (former SLC21) superfamily of transporters. Mol Aspects Med 2013;34:396–412
2. Karlgren M, Vildhede A, Norinder U, et al. Classification of inhibitors of hepatic organic anion transporting polypeptides (OATPs): influence of protein expression on drug-drug interactions. J Med Chem 2012;55:4740–4763
3. Barrera-Hernandez G, Wanke IE, Wong NC. Effects of diabetes mellitus on hepatocyte nuclear factor 1 decrease albumin gene transcription. J Biol Chem 1996;271:9969–9975
4. Dostalek M, Sam WJ, Paryani KR, Macwan JS, Gohh RY, Akhlaghi F. Diabetes mellitus reduces the clearance of atorvastatin lactone: results of a population pharmacokinetic analysis in renal transplant recipients and in vitro studies using human liver microsomes. Clin Pharmacokinet 2012;51:591–606
5. Hagenbuch B, Adler ID, Schmid TE. Molecular cloning and functional characterization of the mouse organic-anion-transporting polypeptide 1 (Oatp1) and mapping of the gene to chromosome X. Biochem J 2000;345:115–120
6. van Montfoort JE, Stieger B, Meijer DKF, Weinmann HJ, Meier PJ, Fattinger KE. Hepatic uptake of the magnetic resonance imaging contrast agent gadoxetate by the organic anion transporting polypeptide Oatp1. J Pharmacol Exp Ther 1999;290:153–157
7. Planchamp C, Hadengue A, Stieger B, et al. Function of both sinusoidal and canalicular transporters controls the concentration of organic anions within hepatocytes. Mol Pharmacol 2007;71:1089–1097
8. Daali Y, Millet P, Dayer P, Pastor CM. Evidence of drug-drug interactions through uptake and efflux transport systems in rat hepatocytes: implications for cellular concentrations of competing drugs. Drug Metab Dispos 2013;41:1548–1556
9. Zhang W, Kong X, Wang ZJ, Luo S, Huang W, Zhang LJ. Dynamic contrast-enhanced magnetic resonance imaging with Gd-EOB-DTPA for the evaluation of liver fibrosis induced by carbon tetrachloride in rats. PLoS One 2015;10:e0129621
10. Tsuda N, Matsui O. Cirrhotic rat liver: reference to transporter activity and morphologic changes in bile canaliculi—gadoxetic acid-enhanced MR imaging. Radiology 2010;256:767–773
11. Byk K, Jasinski K, Bartel Z, et al. MRI-based assessment of liver perfusion and hepatocyte injury in the murine model of acute hepatitis. MAGMA 2016;29:789–798
12. Ulloa JL, Stahl S, Yates J, et al. Assessment of gadoxetate DCE-MRI as a biomarker of hepatobiliary transporter inhibition. NMR Biomed 2013;26:1258–1270
13. Wu Z, Cheng ZL, Yi ZL, et al. Assessment of nonalcoholic fatty liver disease in rats using quantitative dynamic contrast-enhanced MRI. J Magn Reson Imaging 2017;45:1485–1493
14. Chen BB, Hsu CY, Yu CW, et al. Dynamic contrast-enhanced magnetic resonance imaging with Gd-EOB-DTPA for the evaluation of liver fibrosis in chronic hepatitis patients. Eur Radiol 2012;22:171–180
15. Norén B, Forsgren MF, Dahlqvist Leinhard O, et al. Separation of advanced from mild hepatic fibrosis by quantification of the hepatobiliary uptake of Gd-EOB-DTPA. Eur Radiol 2013;23:174–181
16. Lagadec M, Doblas S, Giraudeau C, et al. Advanced fibrosis: correlation between pharmacokinetic parameters at dynamic gadoxetate-enhanced MR imaging and hepatocyte organic anion transporter expression in rat liver. Radiology 2015;274:379–386
17. Giraudeau C, Leporq B, Doblas S, et al. Gadoxetate-enhanced MR imaging and compartmental modelling to assess hepatocyte bidirectional transport function in rats with advanced liver fibrosis. Eur Radiol 2017;27:1804–1811
18. Harris RBS, Zhou J, Redmann SM Jr., et al. A leptin dose-response study in obese (ob/ob) and lean (+/?) mice. Endocrinology 1998;139:8–19
19. Feldman JM, Blalock JA, Foster LB. Effects of food restriction on mice with the hereditary obese-hyperglycemic syndrome. Acta Diabetol Lat 1979;16:27–33
20. Brix AE, Elgavish A, Nagy TR, Gower BA, Rhead WJ, Wood PA. Evaluation of liver fatty acid oxidation in the leptin-deficient obese mouse. Mol Genet Metab 2002;75:219–226
21. Liu W, Struik D, Nies VJ, et al. Effective treatment of steatosis and steatohepatitis by fibroblast growth factor 1 in mouse models of nonalcoholic fatty liver disease. Proc Natl Acad Sci U S A 2016;113:2288–2293
22. Graham DJ, Staffa JA, Shatin D, et al. Incidence of hospitalized rhabdomyolysis in patients treated with lipid-lowering drugs. JAMA 2004;292:2585–2590
23. Thompson PD, Clarkson P, Karas RH. Statin-associated myopathy. JAMA 2003;289:1681–1690
24. Shih DQ, Bussen M, Sehayek E, et al. Hepatocyte nuclear factor-1α is an essential regulator of bile acid and plasma cholesterol metabolism. Nat Genet 2001;27:375–382
25. Lee W, Glaeser H, Smith LH, et al. Polymorphisms in human organic anion-transporting polypeptide 1A2 (OATP1A2): implications for altered drug disposition and central nervous system drug entry. J Biol Chem 2005;280:9610–9617
26. Kullak-Ublick GA, Hagenbuch B, Stieger B, et al. Molecular and functional characterization of an organic anion transporting polypeptide cloned from human liver. Gastroenterology 1995;109:1274–1282
27. Leonhardt M, Keiser M, Oswald S, et al. Hepatic uptake of the magnetic resonance imaging contrast agent Gd-EOB-DTPA: role of human organic anion transporters. Drug Metab Dispos 2010;38:1024–1028
28. Nassif A, Jia J, Keiser M, et al. Visualization of hepatic uptake transporter function in healthy subjects by using gadoxetic acid-enhanced MR imaging. Radiology 2012;264:741–750
29. Pastor CM, Müllhaupt B, Stieger B. The role of organic anion transporters in diagnosing liver diseases by magnetic resonance imaging. Drug Metab Dispos 2014;42:675–684
30. Spinazzi A, Lorusso V, Pirovano G, Kirchin M. Safety, tolerance, biodistribution, and MR imaging enhancement of the liver with gadobenate dimeglumine: results of clinical pharmacologic and pilot imaging studies in nonpatient and patient volunteers. Acad Radiol 1999;6:282–291

31. de Haën C, Lorusso V, Tirone P. Hepatic transport of gadobenate dimeglumine in TR-rats. Acad Radiol 1996;3(Suppl. 2):S452–S454
32. Lorusso V, Arbughi T, Tirone P, de Haën C. Pharmacokinetics and tissue distribution in animals of gadobenate ion, the magnetic resonance imaging contrast enhancing component of gadobenate dimeglumine 0.5 M solution for injection (MultiHance). J Comput Assist Tomogr 1999;23(Suppl. 1):S181–S194
33. Pastor CM, Wissmeyer M, Millet P. Concentrations of Gd-BOPTA in cholestatic fatty rat livers: role of transport functions through membrane proteins. Contrast Media Mol Imaging 2013;8:147–156
34. Hazlehurst JM, Woods C, Marjot T, Cobbold JF, Tomlinson JW. Non-alcoholic fatty liver disease and diabetes. Metabolism 2016;65:1096–1108
35. Cheng Q, Aleksunes LM, Manautou JE, et al. Drug-metabolizing enzyme and transporter expression in a mouse model of diabetes and obesity. Mol Pharm 2008;5:77–91
36. Donepudi AC, Cheng Q, Lu ZJ, Cherrington NJ, Slitt AL. Hepatic transporter expression in metabolic syndrome: phenotype, serum metabolic hormones, and transcription factor expression. Drug Metab Dispos 2016;44:518–526
37. Kulkarni SR, Xu J, Donepudi AC, Wei W, Slitt AL. Effect of caloric restriction and AMPK activation on hepatic nuclear receptor, biotransformation enzyme, and transporter expression in lean and obese mice. Pharm Res 2013;30:2232–2247
38. More VR, Wen X, Thomas PE, Aleksunes LM, Slitt AL. Severe diabetes and leptin resistance cause differential hepatic and renal transporter expression in mice. Comp Hepatol 2012;11:1
39. More VR, Slitt AL. Alteration of hepatic but not renal transporter expression in diet-induced obese mice. Drug Metab Dispos 2011;39:992–999
40. Xu C, Zhu L, Chan T, et al. The altered renal and hepatic expression of solute carrier transporters (SLCs) in type 1 diabetic mice. PLoS One 2015;10:e0120760
41. Zhai T, Wang J, Sun L, Chen Y. The effect of streptozotocin and alloxan on the mRNA expression of rat hepatic transporters in vivo. AAPS PharmSciTech 2015;16:767–770